Grating couplers on porous silicon planar waveguides for sensing applications

X. Wei,[1] C. Kang,[2] M. Liscidini,[3] G. Rong,[1] S. T. Retterer,[4] M. Patrini,[5] J. E. Sipe,[3] and S. M. Weiss[1,2,a)]

[1]*Department of Electrical Engineering and Computer Science, Vanderbilt University, Nashville, Tennessee 37235, USA*
[2]*Interdisciplinary Graduate Program in Materials Science, Vanderbilt University, Nashville, Tennessee 37235, USA*
[3]*Department of Physics and Institute for Optical Sciences, University of Toronto, Toronto, Ontario M5S 1A7, Canada*
[4]*Center for Nanophase Materials Sciences, Oak Ridge National Laboratory, Oak Ridge, Tennessee 37831, USA*
[5]*CNISM and Dipartimento di Fisica "A. Volta," Università degli Studi di Pavia, via Bassi 6, 27100 Pavia, Italy*

We study the use of polymer gratings as light couplers into porous silicon planar waveguides for sensing applications. Experimental evidence of a guided mode in a grating-coupled porous silicon structure is presented, along with a study of its detuning due to waveguide infiltration with a chemical linker. All the measurements are in good agreement with simulations obtained by means of a Fourier modal method, where the porous silicon birefringence is considered. These results demonstrate that this system is potentially useful for chemical and biological sensing applications. © *2008 American Institute of Physics*. [DOI: 10.1063/1.3043579]

I. INTRODUCTION

Porous silicon (PSi) waveguides were first reported more than a decade ago,[1–3] shortly after visible photoluminescence[4] and electroluminescence[5] from PSi films were first demonstrated. Using simple fabrication techniques, PSi waveguides provide a convenient means of guiding light with typical losses ranging from 0.2 to 30 dB/cm, depending on the wavelength and the degree to which the waveguides are oxidized.[1,2,6–14] A PSi slab waveguide can be formed by electrochemically etching a high porosity (low refractive index) layer beneath a low porosity (high refractive index) PSi layer. In this way, light is trapped in the high index layer by total internal reflection at the interfaces with the low index PSi layer below and air above. Strip, buried, and channel waveguides can also be fabricated in PSi using a combination of standard lithographic processing and localized oxidation techniques.[2,10,11,15] While initially proposed for optical interconnections, PSi waveguides have been more recently studied for sensing applications.[16–19]

There are several ways to couple light into a PSi slab waveguide. The most common method employed is end-fire coupling.[20] Light is incident on the end face of the waveguide, often via an optical fiber or by focusing with a microscope objective, and some fraction of the incident light is transmitted directly into the waveguide. Efficient coupling requires a smooth waveguide end face, fine adjustment of the relative positions and sizes of the incident beam and waveguide, and careful mode matching. While much of PSi waveguide research relies on the use of this coupling method, prisms have also been utilized to couple light into PSi waveguides. Light experiences total internal reflection at the base of a glass prism that can be in direct contact with the waveguide silicon substrate (Kretschmann configuration) or a few hundred nanometers above the waveguide core (Otto configuration). When the component of the incident light wave vector in the prism parallel to the interface matches that of a guided mode, evanescent coupling of light into the waveguide core occurs. Prism coupling has been most commonly used to determine the refractive index of PSi layers.[21,22] More recently, prism coupling has been performed for high sensitivity biosensing applications with PSi waveguides.[16,23] Unlike common surface plasmon sensors, optical fiber sensors, and others, such a PSi sensor does not rely on the presence of the target material in an evanescent field; rather, the target is subject to the large propagating field within the waveguide core.[23]

In this work, we show that waveguide mode excitation in a PSi waveguide is possible by means of a photoresist grating that is directly fabricated on the waveguide core by means of electron beam lithography. We note that projection lithography could also be used for the grating fabrication, which would allow for the production of multiple samples on a single wafer. The grating provides the necessary momentum for coupling the incident beam into a guided mode without the need of a prism. We demonstrate that this solution does not impede the use of the structure for sensing applications.

In Sec. II, we discuss the fabrication of planar PSi waveguides and grating couplers. In Sec. III, we begin by presenting the optical characterization of the system before grating fabrication. This is done by means of a reflectance spectrum, which gives information about the actual parameters of the fabricated PSi waveguide and angle-resolved at-

a)Electronic mail: sharon.weiss@vanderbilt.edu.

tenuated total reflectance (ATR) measurements, which allow us to determine the guided mode wave vector. Then reflectance measurements as a function of the incident angle are used to demonstrate guided mode excitation for the grating-coupled PSi waveguide. Finally, in Sec. IV, we present an analysis of the angular shift of the guided mode resonances following infiltration of a chemical linker, 3-aminopropyltriethoxysilane (3-APTES), into the PSi waveguide. This suggests possible applications as a sensor for chemical or biological molecules.

II. FABRICATION

The PSi waveguide is fabricated by electrochemical etching of p^+ (0.01 Ω cm) silicon wafers in a 15% ethanoic hydrofluoric acid electrolyte as previously reported.[16] The PSi waveguide consists of the two following thin PSi films: a top low porosity (high refractive index) layer etched at 5 mA/cm^2 for 62 s and a bottom high porosity (low refractive index) layer etched at 48 mA/cm^2 for 53 s. After anodization, the waveguides are soaked in 1.5 mM KOH for 30 min to widen the pores and then thermally oxidized at 500 °C for 5 min.

Grating structures are fabricated on electrochemically etched PSi using electron beam lithography. A positive e-beam resist, ZEP 520A (Zeon Corp.), is spin coated onto PSi waveguides and then soft baked for 2 min on a 180 °C hot plate. The resulting photoresist films are approximately 400 nm thick. Grating exposures are performed on a JEOL-9300FS electron beam lithography tool at an acceleration voltage of 100 kV and beam current of 2 nA. Completed patterns are developed in xylene solution for 30 s. Inspection of grating structures after fabrication clearly shows intact PSi and with open pores between the grating resist lines. Figure 1 shows scanning electron microscopy (SEM) images of the photoresist gratings and the PSi waveguide. The nominal thicknesses of the PSi waveguide layers, as measured by SEM, are as follows: 325 ± 20 nm top PSi layer and 1500 ± 20 nm bottom layer. The grating period is 1590 ± 10 nm with a duty cycle of approximately 42%.

III. OPTICAL CHARACTERIZATION

The PSi waveguide is characterized by reflectance and angle-resolved ATR measurements before the grating fabrication. These sets of experiments allow verification of the multilayer composition and the effect of the oxidation process on the refractive indices of the layers. The experimental results are compared with theoretical calculations obtained with a Fourier modal method, in which the frequency dependence of the refractive index, absorption, and material birefringence is taken into account.[24] Axial and transversal refractive indices in each PSi layer are evaluated as a function of air and oxide fractions using the model proposed by Lugo *et al.*,[25] in which the refractive indices of silicon and silica are taken from Palik.[26] Note that all the experimental results reported in this work are obtained for an electric field transverse to the plane of incidence (TE) with the sample oriented such that the field is along the grating lines. This means that only the transversal refractive index $n_\perp$ is relevant. The fits
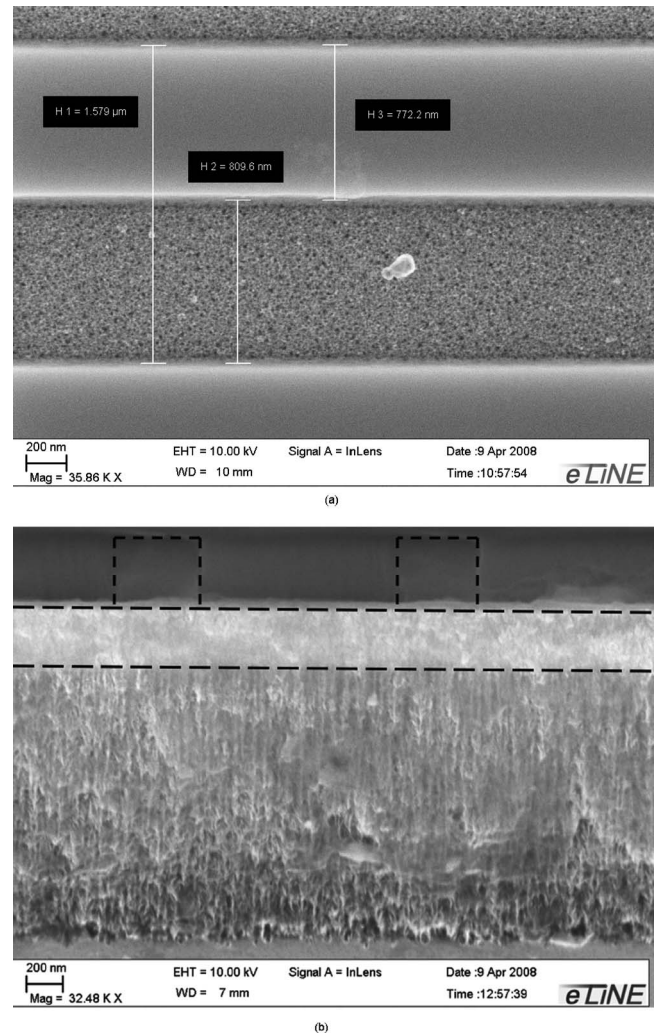

FIG. 1. (a) Top view SEM image of photoresist grating coupler showing photoresist lines with exposed PSi in between the grating lines. (b) Cross-sectional SEM image of grating-coupled PSi waveguide showing core and cladding layers, and photoresist grating above the waveguide. The dotted lines are guides to the eyes.

of the experimental curves are challenging due to the fact that air as well as oxidation fractions have to be determined; moreover, there is a further degree of freedom in that the layer thicknesses can only be roughly estimated using the SEM picture shown in Fig. 1(b).

In Fig. 2 we show the experimental reflectance spectrum of the oxidized multilayer obtained at near-normal incidence using a Varian Cary 5000 UV-visible near-infrared spectrophotometer. Good agreement with the corresponding theoretical curve calculated using the parameters reported in Table I is found for the interference fringe positions, which depend on the layer optical thicknesses. Experimental and theoretical amplitudes of the interference pattern are quite different as the beam frequency increases. This effect can be attributed to sample inhomogeneity and roughness, which lead to an increase in scattering at shorter wavelengths, and to the absorption associated with the *p* doping of the silicon used to fabricate the multilayer. From the best fit, we obtained values for core and buffer layer thicknesses of 340 and 1499 nm,
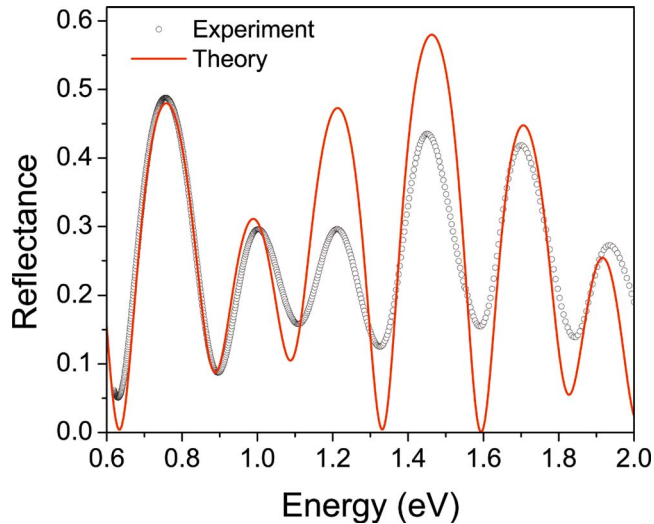
FIG. 2. (Color online) Experimental (points) and theoretical (line) reflectance spectra at normal incidence as a function of the incident beam energy.
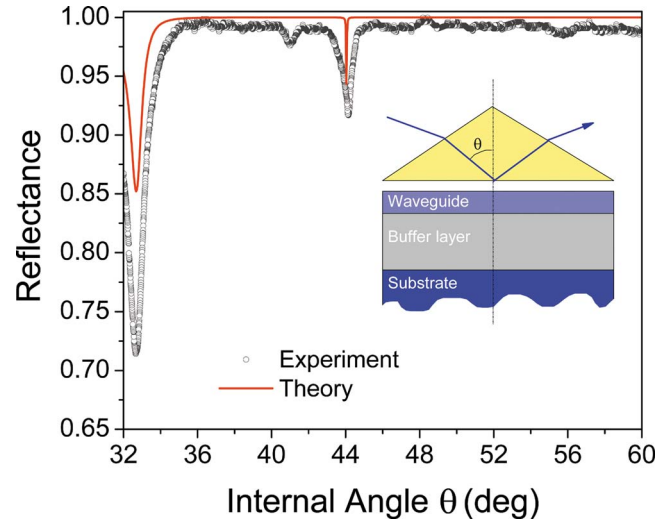

FIG. 3. (Color online) Experimental (points) and theoretical (line) angle-resolved ATR spectra for the PSi waveguide in the case of a TE polarized incident beam. The simulation is done using the structure parameters obtained from the best fit of reflectance spectrum presented in Fig. 2. A scheme of the experimental configuration is also shown.

respectively. These values are compatible with those expected from the etching time and with those estimated from the SEM measurements.

In Fig. 3 we present the angle-resolved ATR measurements obtained by means of a Metricon 2010 prism coupler system, with a rutile prism (n_{prism}=2.1252), in the Otto configuration (see inset) for TE polarized incident light at the wavelength λ=1.55 μm. The prism is placed above the structure a few hundred nanometers from the waveguide surface. Above the critical angle between prism and air, the light is entirely reflected unless it is coupled through the prism into the waveguide. The coupled light can be absorbed, scattered, or even transmitted through the buffer layer into the silicon substrate; thus, for each guided mode, we observe a dip in the reflectance. In particular, the spectrum in Fig. 3 presents a structure that corresponds to the fundamental TE waveguide mode at $\cong$44°. The effective index of the mode is found to be n_{eff}=1.4763, according to the relation n_{eff} =$n_{prism} \sin(\theta_{int})$, where θ_{int} is the angle of incidence measured in the prism. The width of the dip is determined by the overall mode losses; they depend on the distance between the prism and the waveguide, the buffer layer thickness, as well as absorption and scattering within the PSi. In the calculation, the refractive indices at 1.55 μm are taken to be $n_\perp$ $\cong$1.81 for the core and $n_\perp \cong$1.26 for the high porosity layer. They correspond to the porosities and oxidation fractions reported in Table I. The PSi layer oxidation is a necessary process to stabilize and functionalize the waveguide. While

the oxidation reduces the effective index of the structure, a sufficient refractive index contrast is still achievable, which guarantees strong field confinement in the waveguide core. We did not take into account the losses due to the scattering and the small absorption associated with the p doping of the silicon; therefore, while the theoretical position of the dip coincides well with the experimental position, its width is much narrower. The theoretical and experimental curves are in substantially good agreement between 32° and 60°, which is the range permitted by our current experimental configuration. It is worth noting that the simulation is done by simply using the parameters reported in Table I; here, the only new fitting parameter is the distance between the prism and the waveguide, which is found to be 700 nm. This value is sufficiently large that the effective index of the mode estimated from the ATR measurements is indeed that of the unperturbed waveguide.

Once the effective index of the mode is known, it is possible to design a grating to directly couple the light into the waveguide without the need of a prism. The grating provides the momentum to the incident beam to match the mode wave vector, according to

$$\frac{2\pi}{\lambda}n_{ext} \sin \theta \pm m\frac{2\pi}{\Lambda} = \frac{2\pi}{\lambda}n_{eff}, \qquad (1)$$

where n_{ext} is the external medium refractive index, Λ is the grating period, and m is an integer.

In Fig. 4, we plot the experimental and theoretical reflectances of the waveguide after the fabrication of the grating coupler. The ZEP 520A ($n_{ZEP} \cong$1.54) grating has thickness of $h \cong$380 nm, air fraction of $f \cong$0.582, and period of Λ $\cong$1590 nm. This should give a coupling angle around 30° according to Eq. (1). The spectrum is obtained with the Metricon 2010 system used for the ATR measurements. In this configuration the prism is removed from the instrument and the angle-resolved measurements are still performed at λ

TABLE I. Guide core and buffer layer parameters for the oxidized structure. Layer thicknesses have been estimated using SEM pictures and reflectance best fit. Porosities and oxidation degree have been obtained by the reflectance best fit, in which silicon porosity and oxidation are described through the model presented by Lugo *et al.* in Ref. 25.

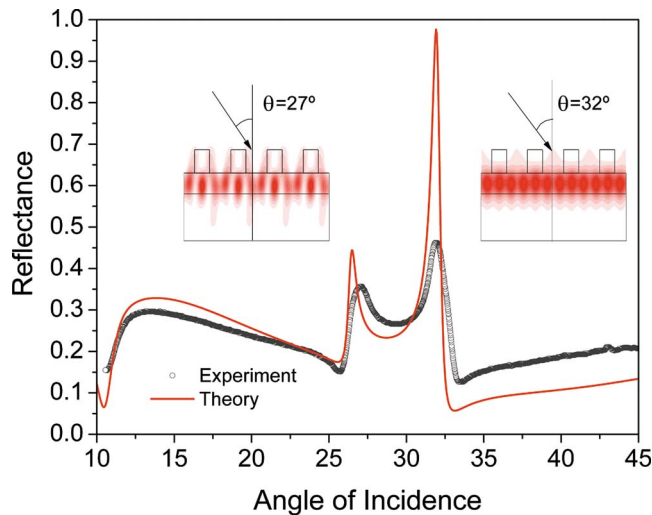| Layer	Thickness (nm)	Percentage of air	Percentage of silicon	Percentage of oxide
Guide	340	61.4	31.3	7.3
Buffer	1499	84.5	8.4	7.1

FIG. 4. (Color online) Experimental reflectance spectrum as a function of the angle of incidence for the PSi waveguide with the grating coupler. The incident beam is TE polarized with wavelength of $\lambda = 1.55$ μm. The calculated field profiles for incident fields at 27° and 32° are also shown.

FIG. 5. (Color online) (a) Measured and (b) calculated angle-resolved reflectance at 1.55 μm (0.8 eV) for empty (solid line) and infiltrated (dashed line) PSi waveguide with a photoresist grating coupler. The incident beam is TE polarized.

$= 1.55$ μm for TE incident light in a range between 10° and 45°. The spectrum is characterized by peaks at 27.1° and 31.9° that result from the light coupling into the multilayer. The angular splitting arises because the grating breaks the continuous translational symmetry of the structure in the waveguide plane. Two field distributions are possible when the guided mode is excited, and two different effective indices result, each with its own associated peak in the spectrum. In particular, when the light is incident at 32°, the field is almost totally confined in the low porosity layer, which is the original waveguide core. When the light is incident at 27°, however, the field extends significantly also into the grating region and the lower cladding where the refractive index is lower. Thus the effective index of this second mode is smaller than that of the first.

IV. EFFECTS OF INFILTRATION

In this section we demonstrate that our structure has potential applications as a refractive index sensor. While guided and surface wave PSi-based sensors have already been proposed,[16,23,27] in our structure the guided modes are excited by means of the grating coupler and not through a prism, leading to a simplification of the detection configuration. Our aim in this first investigation is to show that the grating fabrication on a PSi structure does not prevent its infiltration, and thus its implementation as a sensing device. Our sensing experiment is based on the fact that PSi infiltration typically leads to modification of the porous layer effective index. This results in a modification of the waveguide mode dispersion and an angular shift of the resonances associated with mode excitation.

In order to test the structure, we study the effects of infiltration with 3-aminopropyltriethoxysilane (3-APTES), which contains an amino group and is commonly used in sensing applications to promote adhesion between silica substrates and organic materials. Once the amine is available, numerous cross-linking agents can be used to immobilize
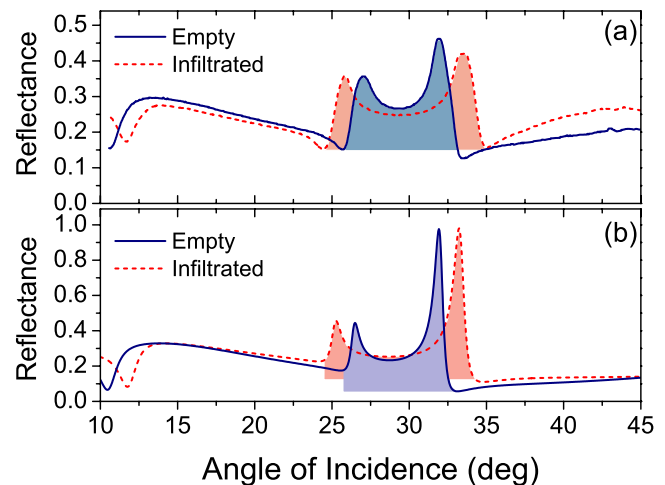
proteins, DNA, or other molecules to silica surfaces. To form a 3-APTES thin film on the PSi pore walls, 100 μl of 4% 3-APTES solution $[3-\mathrm{APTES}(99\%,\mathrm{Aldrich}):\mathrm{methanol}:\mathrm{de\text{-}ionized\ water}=4:46:50]$ were dropped on the grating sample's surface. After incubation in a humid environment for 20 min, the sample was rinsed with de-ionized water, dried with nitrogen, and baked at 100 °C for 10 min. In Fig. 5(a) we show the experimental reflectance spectra of the grating-coupled waveguide before and after the infiltration. The infiltration leads to the formation of an almost atomic layer of 3-APTES on the surface of the PSi pores and to an increase in the refractive index in the waveguide core and buffer layers in the regions that are not covered by photoresist. As a consequence of the increase in refractive index, the resonance splitting is enhanced. The shifted peaks are at 25.8° and 33.6°, respectively, for a total splitting of 7.7°, which is almost 3° larger than what is observed with the empty waveguide. Each resonance peak shifts about half of the total splitting.

We use our theoretical model to confirm that the splitting can indeed be understood as due to the infiltration of the waveguide. Since the 3-APTES refractive index is almost identical to that of silica, we can still use the model of Lugo *et al.*[25] to calculate the effective refractive index change by simply adjusting the air fraction to take into account the infiltration. In Fig. 5(b), we plot the calculated reflectance spectra for the empty and infiltrated structures. We find a good agreement with the experimental results when we assume refractive index changes $\Delta n_{\perp,\mathrm{core}} = 0.033\,51$ and $\Delta n_{\perp,\mathrm{buffer}} = 0.037\,69$ in the core and buffer layers, respectively.

If we compare the angular shift of the resonance associated with the mode guided completely in the waveguide core for the current grating-coupled and previously reported prism-coupled[16] configurations, we find that the magnitude of the shift due to 3-APTES infiltration is nearly the same in both cases. However, for the grating-coupled waveguides, only half of the sensing region is usable due to the presence of the photoresist gratings. This implies that higher sensitivi-

ties could be obtained if the entire sensing area were infiltrated, for example, by fabricating the grating directly in the PSi material. It is also noteworthy that since the grating-coupled waveguide produces two resonance peaks, an easier means of detection would be to monitor the change in peak splitting. Since the two resonance peaks shift in opposite directions, the magnitude of the splitting change is twice that of a single resonance shift.

V. CONCLUSION

We have proposed a polymer grating for the compact and efficient coupling of light into a PSi planar waveguide. The optical properties of the waveguide have been studied by angle-resolved ATR measurements, which allow accurate determination of an appropriate grating period for efficient coupling of light into the waveguide. A ZEP 520A photoresist grating has been fabricated on the PSi waveguide using standard electron beam lithography, and the system has been characterized by angle-resolved reflectance. We experimentally verified that such a device can be used as a refractive index sensor, where mode coupling is obtained by means of the grating instead of a prism. All measurements are in good agreement with theoretical calculations. These results demonstrate the potential usefulness of this system for chemical and biological sensing applications.

ACKNOWLEDGMENTS

[1] V. P. Bondarenko, A. M. Dorofeev, and N. M. Kazuchits, Microelectron. Eng. **28**, 447 (1995).
[2] A. Loni, L. T. Canham, M. G. Berger, R. Arens-Fischer, H. Munder, H. Luth, H. F. Arrand, and T. M. Benson, Thin Solid Films **276**, 143 (1996).
[3] L. Pavesi, Riv. Nuovo Cimento **20**, 1 (1997).
[4] L. T. Canham, Appl. Phys. Lett. **57**, 1046 (1990).
[5] N. Koshida and H. Koyama, Appl. Phys. Lett. **60**, 347 (1992).
[6] G. Amato, L. Boarino, S. Borini, and A. M. Rossi, Phys. Status Solidi A **182**, 425 (2000).
[7] H. F. Arrand, T. M. Benson, A. Loni, M. G. Krueger, M. Thoenissen, and H. Lueth, Electron. Lett. **33**, 1724 (1997).
[8] G. Maiello, S. LaMonica, A. Ferrari, G. Masini, V. P. Bondarenko, A. M. Dorofeev, and N. M. Kazuchits, Thin Solid Films **297**, 311 (1997).
[9] P. Ferrand and R. Romestain, Appl. Phys. Lett. **77**, 3535 (2000).
[10] J. Charrier, C. Lupi, L. Haji, and C. Boisrobert, Mater. Sci. Semicond. Process. **3**, 357 (2000).
[11] A. M. Rossi, G. Amato, V. Camarchia, L. Boarino, and S. Borini, Appl. Phys. Lett. **78**, 3003 (2001).
[12] N. Vorozov, L. Dolgyi, V. Yakovtseva, V. Bondarenko, M. Balucani, G. Lamedica, A. Ferrari, G. Vitrant, J. E. Broquin, T. M. Benson, H. F. Arrand, and P. Sewell, Electron. Lett. **36**, 722 (2000).
[13] P. Pirasteh, J. Charrier, Y. Dumeige, S. Haesaert, and P. Joubert, J. Appl. Phys. **101**, 083110 (2007).
[14] M. Balucani, V. Bondarenko, A. Klusko, and A. Ferrari, Opt. Mater. (Amsterdam, Neth.) **27**, 776 (2005).
[15] M. Takahashi and N. Koshida, J. Appl. Phys. **86**, 5274 (1999).
[16] G. Rong, A. Najmaie, J. E. Sipe, and S. M. Weiss, Biosens. Bioelectron. **23**, 1572 (2008).
[17] H. F. Arrand, T. M. Benson, A. Loni, R. Arens-Fischer, M. Kruger, M. Thonissen, H. Luth, and S. Kershaw, IEEE Photonics Technol. Lett. **10**, 1467 (1998).
[18] P. Rivolo, P. Pirasteh, A. Chaillou, P. Joubert, M. Kloul, J. F. Bardeau, and F. Geobaldo, Sens. Actuators B **100**, 99 (2004).
[19] H. F. Arrand, T. M. Benson, A. Loni, R. Arens-Fischer, M. G. Krueger, M. Thoenissen, H. Lueth, S. Kershaw, and N. N. Vorozov, J. Lumin. **80**, 119 (1998).
[20] E. Gizeli and C. R. Lowe, *Biomolecular Sensors* (Taylor & Francis, London, 2002).
[21] I. Mihalcescu, G. Lerondel, and R. Romestain, Thin Solid Films **297**, 245 (1997).
[22] J. Charrier, E. Le Gorju, L. Haji, and M. Guendouz, J. Porous Mater. **7**, 243 (2000).
[23] J. J. Saarinen, S. M. Weiss, P. M. Fauchet, and J. E. Sipe, Opt. Express **13**, 3754 (2005).
[24] M. Liscidini, D. Gerace, L. C. Andreani, and J. E. Sipe, Phys. Rev. B **77**, 035324 (2008).
[25] J. E. Lugo, H. A. Lopez, S. Chan, and P. M. Fauchet, J. Appl. Phys. **91**, 4966 (2002).
[26] E. D. Palik, *Handbook of Optical Constants of Solids* (Academic, Orlando, FL, 1985).
[27] E. Guillermain, V. Lysenko, R. Orobtchouk, T. Benyattou, S. Roux, A. Pillonnet, and P. Perriat, Appl. Phys. Lett. **90**, 241116 (2007).